JOURNAL OF GEOPHYSICAL RESEARCH, VOL. ???, XXXX, DOI:10.1029/,

Relation of Cloud Occurrence Frequency, Overlap, and Effective Thickness Derived from CALIPSO and CloudSat Merged Cloud Vertical Profiles

Seiji Kato,[1] Sunny Sun-Mack,[2] Walter F. Miller,[2] Fred G. Rose,[2] Yan Chen,[2]

Patrick Minnis,[1] and Bruce A. Wielicki[1]

Seiji Kato, Climate Science Branch, NASA Langley Research Center Hampton, Virginia 23681-2199, USA. (seiji.kato@nasa.gov)

[1]Climate Science Branch, NASA Langley Research Center, Hampton, Virginia, USA.

[2]Science Systems and Applications, Inc., Hampton, Virginia, USA.

Abstract. A cloud frequency of occurrence matrix is generated using merged cloud vertical profile derived from Cloud-Aerosol Lidar with Orthogonal Polarization (CALIOP) and Cloud Profiling Radar (CPR). The matrix contains vertical profiles of cloud occurrence frequency as a function of the uppermost cloud top. It is shown that the cloud fraction and uppermost cloud top vertical profiles can be related by a set of equations when the correlation distance of cloud occurrence, which is interpreted as an effective cloud thickness, is introduced. The underlying assumption in establishing the above relation is that cloud overlap approaches the random overlap with increasing distance separating cloud layers and that the probability of deviating from the random overlap decreases exponentially with distance. One month of CALIPSO and CloudSat data support these assumptions. However, the correlation distance sometimes becomes large, which might be an indication of precipitation. The cloud correlation distance is equivalent to the de-correlation distance introduced by *Hogan and Illingworth* [2000] when cloud fractions of both layers in a two-cloud layer system are the same.

1. Introduction

An accurate characterization of the vertical profiles of cloud properties for both single-layered and overlapping clouds is critical for calculating the radiative flux divergence within in and at the top of the atmosphere. For example, *Barker et al.* [2003] demonstrated that, for a given vertical distribution of liquid water content, changing the cloud overlap conditions can introduce errors in the zonal annual mean top-of-atmosphere (TOA) cloud radiative effect by up to 50 Wm^{-2}. Estimating the cloud base height accurately is important for surface radiation budget computations especially in polar regions. For example, simply changing the base height of an optically thick cloud from 5 km to 1 km increases the downward longwave irradiance by nearly 10%. In addition to the importance of cloud overlap to radiation, cloud overlap affects precipitation parameterization in general circulation models (GCMs). If precipitation falls through clouds, collision and coalescence need to be considered but for precipitation falling through cloud-free air, evaporation needs to be considered [*Jacob and Klein*, 2000].

Multi-layer cloud information is not available from cloud retrievals by passive sensors except when a thin layer overlapping with optically thick warm clouds [*Chang and Li*, 2005]. In addition, undetected thin cirrus sometimes causes an error in cloud height retrieval if it overlaps with low-level clouds. In this case, a retrieval algorithm tends to place the cloud top in between the two cloud tops. Additionally, retrievals of total cloud water path tend to be biased when an ice cloud overlaps a liquid water cloud [*Minnis et al.*, 2007]. New active sensors, however, are now providing multi-layer cloud information lacking in previous satellite measurements. The Cloud-Aerosol Lidar and Infrared Pathfinder Satellite

Observation (CALIPSO) satellite and CloudSat provide detailed data on the vertical profile of clouds from the Tropics to polar regions. The CALIPSO Cloud-Aerosol Lidar with Orthogonal Polarization (CALIOP) and CloudSat Cloud Profiling Radar (CPR) identify multi-layered cloud top and base heights that are not easily detected with passive sensors.

In earlier studies, *Hogan and Illingworth* [2000] derived cloud overlap statistics from ground-based radar data. They used the variable α that linearly combines the random and maximum cloud overlap. They assume that α decreases exponentially as the separation between two cloud layers increases and define the e-folding distance (or de-correlation distance). *Wang and Dessler* [2006] used 20 days of Ice, Cloud,and land Elevation Satellite (ICESat) data over the Tropics to show that 1/3 of boundary layer clouds overlap nearly randomly with cirrus clouds. *Mace and Benson-Troth* [2002] extended the work of *Hogan and Illingworth* [2000] and derived seasonal and regional variations of α and its e-folding length using ground-based Atmospheric Radiation Measurement (ARM) radar data taken at 4 different sites. *Barker* [2008b] derived α from 2 months of CPR and CALIOP combined data and found that, over Southern Great Plains (SGP) ARM site, the de-correlation distance is consistent with that reported by *Mace and Benson-Troth* [2002].

A first step in using multi-layer cloud information from CALIOP and CPR is to merge cloud vertical profiles (hereinafter merged cloud profiles) derived independently from two instruments. Cloud profiles from either CALIPSO or CloudSat alone are not enough to provide a complete picture of cloud vertical profiles; The CPR tends to miss thin clouds composed of small cloud particles (the minimum detection is -30 dBZ, *Stephens et al.* [2008]) and CALIOP signal is attenuated by optically thick clouds (optical thickness

greater than about 3). Section 2 discusses our method of merging cloud profiles derived from CALIOP and CPR.

Once cloud profiles from the two instruments are merged, the impact of cloud structures on the irradiance profiles can be assessed by comparing the irradiances computed with merged cloud profiles to those computed using simple single-layer clouds, which are the typical products retrieved from passive sensor measurements. For this reason, we will further collocate merged cloud profiles with footprints of the Clouds and the Earth's Radiant Energy System (CERES) instrument on*Aqua*. In addition, radiative effects at the surface and in the atmosphere are evaluated when irradiance vertical profiles are computed by a radiative transfer model using merged cloud vertical profiles. Aiming toward this goal, we keep cloud information at the original CALIOP and CPR resolutions as much as possible while collocating and merging them into CERES footprints so that the independent column approximation can be properly applied in computing the irradiance profile. One purpose of this paper is to describe the process to merge CALIOP and CPR derived cloud profiles within a CERES footprint. Although this study does not use the result of collocation of cloud profiles with CERES footprints and CERES-derived irradiances, this paper includes descriptions of the process in the Appendix A because the process is interwoven with the CALIOP and CPR cloud profile merging process.

The main purpose of this paper is to describe a tool to quantitatively analyze cloud vertical profiles in order to assess their impact on radiation. Our approach to quantitatively evaluate vertical cloud profiles and overlap is different that introduced by *Hogan and Illingworth* [2000]. We sort merged cloud profiles and form a simple cloud frequency of occurrence matrix. The matrix leads to a set of equations that relates the cloud frac-

tion exposed to space, cloud fraction vertical profile and cloud physical thickness. For a two-layer cloud system under a certain condition, the de-correlation length introduced by *Hogan and Illingworth* [2000] can be related to the cloud effective thickness. The relation between cloud fraction, topmost cloud top vertical profiles, and cloud thickness, therefore, provides a physical interpretation of the de-correlation length, a parameter that appears somewhat unique to GCMs. In this paper, we only treat correlations of cloud mask and did not consider correlation of liquid or ice water content as done by *Hogan and Illingworth* [2003].

Section 2 describes the process combining CALIOP and CPR derived cloud profiles, Section 3 introduces the cloud frequency of occurrence matrix, derives a set of equations relating the cloud occurrence, uppermost cloud top, and cloud thickness, and discusses the relation of our approach to the concept introduced by *Hogan and Illingworth* [2000].

2. CALIPSO and CloudSat combined cloud profile

The CALIPSO program provides the Vertical Feature Mask (VFM), which defines clouds and aerosols at a , 0.333-km horizontal resolution below 8.2 km altitude and a 1-km horizontal resolution above 8.2 km [*Winker et al.,* 2007]. The CloudSat CLDCLASS data provide information on clouds at a 1.4-km cross-track horizontal resolution and at a range, or vertical, resolution of 480 m *Stephens et al.* [2008]. To take advantage of both the CALIOP and CPR instruments, first, the VFM and CLDCLASS profiles are collocated using 1-km $\times$ 1-km grids. Second, the combined cloud profiles are collocated with CERES footprints, which are approximately 20 km in size. Note that the actual point spread function of the CERES instruments is approximately 35 km in size because

the response time causes a widening and skewing the point spread function [*Smith*, 1994]. Third, based on the cloud top and base heights, the cloud profiles that fall within a CERES instrument footprint are grouped together in the following way.

Every 1-km by 1-km grid box contains one CloudSat and three VFM vertical profiles. Each CALIPSO-derived cloud profile is compared with a collocated CloudSat-derived cloud profile to combine the information. The cloud top and base heights for the grid box are determined using the strategy described in Table 1. Because the CloudSat range resolution is greater than CALIPSOs, the CALIOP and CPR derived cloud boundaries need to differ more than 480 m to be considered as distinctly different boundaries. The merged cloud profiles are primarily based on CALIOP derived cloud profiles, except when the signal is completely attenuated. About 85% of cloud tops and 77% of cloud bases of merged profiles are derived from CALIOP data. When the CPR identifies a cloud boundary that is more than 480 m away from CALIOP-derived cloud boundary, the cloud boundary is inserted to the CALIOP derived cloud profile. Cloud bases are from CALIOP data (Table 1) to avoid the influence of precipitation. In a a very few cases, CALIOP did not detect clouds in the height range between CPR-detected cloud top and base. A CPR-detected cloud layer is then inserted for this case.

We determined the maximum number of groups allowed within a CERES footprint is 16 and the maximum number of layers allowed within a group is 6 after reviewing statistics of the number of unique cloud groups within a footprint and cloud layers in the profile. For the cases when the number of unique groups exceeded sixteen, the process explained in Appendix C was adopted to combine profiles with nearly the same cloud top and base heights. Those grouped cloud profiles are used in this study. Because this cloud grouping

process only change the order of occurrence of cloud profiles within approximately 35 km, imposing the size of CERES footprint as a domain to form cloud groups does not degrade the original cloud vertical profile information observed by CALIOP and CPR, except for profiles that exceed the limit of 16 groups within the domain.

3. Cloud Frequency of Occurrence Matrix

To form a cloud frequency of occurrence matrix, we sort merged cloud vertical profiles explained in the previous section by the uppermost cloud top height z_{top} with the bin size of 200 m and count the number of cloud occurrence below the uppermost cloud top. This process produces a 2D histogram of cloud occurrence of which columns are separated by the highest cloud top z_{top} and rows contain the vertical profile of cloud occurrence for a given uppermost cloud top. The element defined by the ith column and jth row, therefore, contains the number of cloud occurrences in the jth layer when the uppermost cloud top height is at the ith layer $z_{top,i}$. When the number of counts in the jth row and ith column is n_{ji}, the probability of cloud occurrence in the jth layer with the uppermost cloud top at the ith level is

$$P(z_j, z_{top,i}) = n_{ji}/N, \tag{1}$$

where N is the total number of profiles, including cloud-free profiles. The cloud layer index starts from the surface and increases with altitude so that

$$n_{ji} \geq 0 \quad when \quad j \leq i, \quad and \quad n_{ji} = 0, \quad when \quad j > i. \tag{2}$$

Therefore, the cloud frequency of occurrence matrix is a lower triangular matrix. It is different from the cloud overlap matrix defined by Willén et al. (2005) in which elements are cloud fraction exposed to space by a two-cloud layer system. The uppermost cloud

layers, which are the diagonal elements of the cloud occurrence frequency matrix, are the clouds exposed to space. The probability of the cloud occurrence in the ith uppermost layer is $P(z_i, z_{top,i})$. The sum of all of the uppermost cloud layers computed over a region over a given period defines the mean cloud fraction

$$C = \frac{\sum_{i=1}^{m} n_{ii}}{N} = \sum_{i=1}^{m} P(z_i, z_{top,i}), \tag{3}$$

where m is the total number of vertical layers. The conditional probability that clouds are present in the jth layer when the uppermost cloud top height is $z_{top,i}$ is

$$P(z_j|z_{top,i}) = \frac{P(z_j, z_{top,i})}{P(z_i, z_{top,i})}, \tag{4}$$

and $P(z_i|z_{top,i}) = 1$. The frequency of cloud occurrence in the jth layer with any uppermost cloud top heights (i.e. the probability of cloud occurrence in the jth layer regardless of cloud occurrence above) is

$$P(z_j) = \frac{\sum_{i=j}^{m} n_{ji}}{N} = \sum_{i=j}^{m} P(z_j, z_{top,i}). \tag{5}$$

Note that the probability of cloud occurrence depends on the vertical depth of the bin (Appendix A). In this study, we use a bin that is sufficiently smaller than the thickness of cloud.

With the above definitions, the random overlap probability of a cloud in the jth layer and ith layer is $P_{z_j} P_{z_i}$. The random overlap probability between clouds at the jth layer and a uppermost cloud top layer at $z_{top,i}$ is $P(z_j)P(z_i, z_{top,i})$. The conditional probability of random overlap of jth layer clouds with an uppermost cloud top is at $z_{top,i}$ is, therefore,

$$P_{rdm}(z_j|z_{top,i}) = P(z_j)P(z_i, z_{top,i})/P(z_i, z_{top,i}) = P(z_j). \tag{6}$$

We further divide the conditional probability $p(z_j|z_{top,i})$ into two terms,

$$P(z_j|z_{top,i}) = \frac{P(z_j, z_{top,i})}{P(z_i, z_{top,i})} = P_{rdm}(z_j|z_{top,i}) + \Delta P(z_j|z_{top,i}), \tag{7}$$

where $P_{rdm}(z_j|z_{top,i})$ is the probability of random overlap defined by (6), and ΔP is the deviation from the random overlap. Therefore,

$$\Delta P(z_j|z_{top,i}) = \frac{P(z_j, z_{top,i})}{P(z_i, z_{top,i})} - P(z_j). \tag{8}$$

When $j = i$,

$$\Delta P(z_i|z_{top,i}) = 1 - P(z_i). \tag{9}$$

Similar to the assumption made in earlier studies (e.g. *Hogan and Illingworth* [2000]), when $i \leq j$, we assume that ΔP decreases exponentially with distance,

$$\Delta P(z_j|z_{top,i}) \approx [1 - P(z_i)] \exp(-\Delta z_{ji}/D_i), \tag{10}$$

where Δz_{ji} is the distance from the ith uppermost cloud top to the ith layer, $z_{top,i} - z_j$, and D is the e-folding distance or correlation length of cloud occurrence, namely the vertical distance that the probability of cloud occurrence that deviates from the random overlap diminishes by a factor of e. Note that the subscript of D indicates that the correlation length is a function of the uppermost cloud top height.

When $\Delta z = 0$ and (10) is substitute in to (7), we recover $P(z_i|z_{top,i}) = 1$, provided $P_{rdm}(z_i|z_{top,i}) = P(z_i)$. The conditional probability of overlap with itself is 1. Therefore $1 - P(z_i)$ in (10) is the conditional probability of the ith layer cloud overlapping the ith layer uppermost cloud top that deviates from the random overlap. If there is no physical process connecting two layers, we would expect that the clouds in those two layers overlap randomly. Therefore, the e-folding distance D_i can be interpreted as the distance over

which the physical process of cloud formation falls off by a factor of e or simply the effective thickness of cloud.

Equation (a5) in Appendix A suggests that the necessary condition to establish the relation of exponential decay is a smaller vertical bin size compared with D. For simplicity, we fix the bin size to 200 m throughout the atmosphere in this study. Our bin size exceeds the 90 m used by earlier study used *Mace and Benson-Troth* [2002]. When D is the effective thickness of clouds, D derived from data does not depend on the bin size as long as the bin size is smaller than D.

Given the uppermost layer at the ith layer, probability of cloud occurrence at the jth layer is, therefore,

$$P(z_j|z_{top,i}) = P(z_j) + [1 - P(z_i)] \exp[-(z_i - z_j)/D_i]. \quad (11)$$

The cloud occurrence in the jth layer is, therefore, obtained by multiplying (11) by $P(z_i, z_{top,i})$ and summing all uppermost cloud top layers above the jth layer,

$$P(z_j)[1 - \sum_{i=j+1}^{m} P(z_i, z_{top,i})] = P(z_j, z_{top,j}) + \sum_{i=j+1}^{m} P(z_i, z_{top,i})[1 - P(z_i)]e^{-(z_i - z_j)/D_i}, \quad (12)$$

where m is the highest cloud layer detected by CALIOP and CPR (See Appendix B for the derivation). When we obtain (12) for all layers, they can be expressed as a matrix operation

$$\mathbf{P} = \mathbf{DT}, \quad (13)$$

where

$$\mathbf{P} = [P(z_1), P(z_2) \cdots P(z_m)]^T, \quad (14)$$

$$\mathbf{T} = [P(z_1, z_{top,1}), P(z_2, z_{top,2}) \cdots P(z_n, z_{top,n})]^T, \quad (15)$$

$$\mathbf{D} =$$

$$\begin{pmatrix} \frac{1}{1-\sum_{i=2}^{m} P(z_i,z_{top,i})} & \frac{[1-P(z_2)]e^{-\frac{z_2-z_1}{D_2}}}{1-\sum_{i=2}^{m} P(z_i,z_{top,i})} & \cdots & \frac{[1-P(z_{m-1})]e^{-\frac{z_{m-1}-z_1}{D_{m-1}}}}{1-\sum_{i=2}^{m} P(z_i,z_{top,i})} & \frac{[1-P(z_m)]e^{-\frac{z_m-z_1}{D_m}}}{1-\sum_{i=2}^{m} P(z_i,z_{top,i})} \\ 0 & \frac{1}{1-\sum_{i=3}^{m} P(z_i,z_{top,i})} & \cdots & \frac{[1-P(z_{m-1})]e^{-\frac{z_{m-1}-z_2}{D_{m-1}}}}{1-\sum_{i=3}^{m} P(z_i,z_{top,i})} & \frac{[1-P(z_m)]e^{-\frac{z_m-z_2}{D_m}}}{1-\sum_{i=3}^{m} P(z_i,z_{top,i})} \\ \vdots & \vdots & \ddots & \vdots & \vdots \\ 0 & 0 & \cdots & \frac{1}{1-\sum_{i=n-1}^{m} P(z_i,z_{top,i})} & \frac{[1-P(z_m)]e^{-\frac{z_m-z_{n-1}}{D_m}}}{1-\sum_{i=n-1}^{m} P(z_i,z_{top,i})} \\ 0 & 0 & \cdots & 0 & 1 \end{pmatrix}, \tag{16}$$

and super script T denotes the transpose of the matrix. In (14), (15), and (16), m is the number of cloud layers, n is the number of uppermost cloud layer, and $n = m$. Equation (13) relates the cloud fraction profile, the uppermost cloud top profile (i.e. the cloud fraction exposed to space) and cloud effective thickness. The matrix $\mathbf{D}$ that relates cloud fraction and uppermost cloud top profiles contains both unknowns but since it is an upper triangular matrix, if either the cloud fraction or the uppermost cloud top vertical profile is known, it can be solved for the other unknown profile provided the correlation length is known. To solve the set of equations, we need to start from the highest layer by setting,

$$P(z_m, z_{top,m}) = P(z_m). \tag{17}$$

Therefore, if the cloud vertical correlation length as a function of uppermost cloud top height is known, vertical cloud fraction and uppermost cloud top profile can be related.

In earlier studies (*Hogan and Illingworth* [2000]; *Bergman and Rasch* [2002]; *Barker* [2008]) the cloud fraction exposed to space for a two-cloud layer system is written as

$$C_{kl} = C_{rdm} - \alpha(C_{rdm} - C_{max}), \tag{18}$$

where C_{rdm} and C_{max} are, respectively, the cloud fraction given by the random and maximum overlap assumptions. This can be written with the notation used here as

$$C_{kl} = P(z_l) + P(z_k) - P(z_k)P(z_l) - \alpha P(z_l)\left[\frac{min[P(z_k), P(z_l)]}{P(z_l)} - P(z_k)\right], \tag{19}$$

where the layer l is the upper layer, $min[P(z_k), P(z_l)]$ is equal to the smaller value between $P(z_k)$ and $P(z_l)$ and $\alpha = e^{\frac{-z_k - z_l}{\Delta z_0}}$.

For a two-cloud layer system, the cloud fraction in two cloud layers, k and l, using the correlation length is the sum of cloud fractions in the upper and lower layers,

$$C_{kl} = P(z_l) + P(z_k) - P(z_k)P(z_l) - P(z_l)[1 - P(z_l)]e^{-\frac{z_k - z_l}{D_k}}. \quad (20)$$

The last term on the right side in both (19) and (20) reduce the cloud fraction exposed to space from that given by the random overlap assumption. Cloud fractions exposed to space computed by (19) and (20) differ for an arbitrary set of two-layer cloud fractions when the distance between two layers is small. The cloud fractions given by (19) and (20) are equal when $P(z_l) = P(z_k)$. Therefore, when $\alpha = e^{-(z_l - z_k)/\Delta z_0}$, our correlation length of D is equivalent to the de-correlation length Δz_0 when $P(z_k) = P(z_l)$. Note that even when the distance between the two layers approaches zero, C_{kl} by (20) does not approach the upper layer cloud fraction unless the cloud fraction in the upper and lower layers are the same. We expect that the cloud fraction difference in upper and lower layer is small when the distance between the cloud layer is small and the difference approaches zero as the distance decreases because of the finite thickness of clouds.

4. Results and Discussion

Figures 1 and 2 show, respectively, the vertical profile of cloud fraction $P(z)$ and $\Delta P(z|z_{top})$ in (7) derived from 1 month of data (July 2006) taken over 6 different regions. $\Delta P(z|z_{top})$ decreases monotonically with the distance from the uppermost cloud top for a given uppermost cloud top height. When the distance is large, it sometimes is negative in the southern hemisphere tropics. One possible reason for this is that the

CALIOP signal is sometimes completely attenuated while the CPR misses low-level clouds so that low-level clouds occur less often than random overlap when mid and high level clouds are present. Note that a large cloud fraction above the tropopause over the Antarctic is in the original CALIPSO VMF data product and results for two reasons (D. Winker personal communication 2009). First, it is sometimes difficult to identify the exact height of tropopause over the Antarctica, and second, clouds that extend from the troposphere into stratosphere are included in VFM data.

The assumption made in the previous section in deriving (12) is that ΔP in (7) decreases exponentially with distance from the uppermost cloud top. Figure 3 shows ΔP as a function of the distance from the uppermost cloud top for selected uppermost cloud top heights. It indicates that ΔP decreases nearly exponentially with distance from the uppermost cloud top for intermediate distance. A large correlation distance, hence a smaller slope such as the 8.9 km case at the greater than 4 km from the uppermost cloud top on the left side plot of Figure 3, might be an indication of precipitation. A small slope near the cloud top might be caused by the finite thickness of clouds i.e. existence of a minimum cloud thickness.

Because the inverse of the slopes of the lines shown in Figure 3 is the correlation distance, the correlation distance as a function of the uppermost cloud top height can be derived by a linear regression. However, Figure 3 indicates that the slope is not constant throughout the atmospheric column for a given uppermost cloud top. Therefore, applying a linear regression to the uppermost cloud top to the surface can leads to a biased estimate. To reduce the error, we compute the slope using a 1.2-km moving window and average all slopes so that a constant slope extending over the largest vertical length is

given the greatest weight. The result is plotted on Figure 4. As expected, the correlation distance, which is the effective cloud thickness, increases with uppermost cloud top height. When the uppermost cloud top height is larger than about 8 km, the correlation distance becomes nearly constant and does not increase with height. This might be caused by frequently occurring thin cirrus. The correlation length in the Tropics does not differ from midlatitude values, probably because thick convective clouds does not occur frequently even in the tropics compared with the occurrence of other cloud types [*Dong et al.* 2008].

The correlation distance derived here is related to the de-correlation length introduced by *Hogan and Illingworth* [2000] as indicated by (19) and (20). Those are not exactly the same but the de-correlation distance, property which appears unique to GCMs, coincides with the correlation distance of clouds defined in this paper when the cloud fraction of two layers in the system are equal. Therefore, this result provides a physical interpretation of the de-correlation distance, which might give some insight into how it is derived and how it can be approximated when it is applied. *Barker* [2008a] speculates that the de-correlation length depends on altitude. Because the above result indicates that the de-correlation length is related to the effective cloud thickness and clearly the cloud thickness depends on cloud type, we expect that the de-correlation length also depends on height.

The height dependence of the de-correlation distance is sometimes neglected when parameterizing the cloud overlap [*Barker* 2008a, *Barker and Päisänen* 2005]. The error in the zonal and monthly mean TOA shortwave irradiance caused by neglecting the height dependence of the de-correlation distance in computing the TOA shortwave irradiance is less than 3 Wm^{-2} [*Barker* 2008a]. If the difference between the de-correlation distance and the correlation distance gives a smaller TOA irradiance change compared with the

TOA irradiance change caused by neglecting height dependence of the de-correlation distance, the cloud correlation distance introduced here might be used as the de-correlation distance for a cloud overlap parameterization.

To obtain a rough estimate of the sensitivity of the TOA reflected shortwave irradiance to the correlation distance, we use (12) and take a derivative with respect to D,

$$\frac{\partial P(z_k, z_{top,k})}{\partial D_l} = -\frac{z_l - z_k}{D_l^2} P(z_l, z_{top,l})[1 - P(z_l)]e^{-(z_l - z_k)/D_l}, \tag{21}$$

where the layer l is the upper layer. The actual cloud fraction in a layer depends on the vertical depth of the layer, but Figure 1 suggests that $P(z_l, z_{top,l}) = P(z_l) \approx 0.25$ can be used as a rough estimate. If we further assume that $D_l = 2$ km, and $z_l - z_k = 2$ km, a 0.5 km error in D_l gives about a 0.1 cloud fraction error in $P(z_k, z_{top,k})$. If we use a typical value of $\approx -40\mathrm{Wm}^{-2}$ for a zonal mean TOA shortwave cloud forcing in the Tropics and 0.6 for a zonal mean cloud fraction exposed to space (e.g. *Kato et al.* [2008]), a 0.1 cloud fraction change gives about 7 Wm^{-2} difference at TOA. Therefore, a rough estimated tolerance of the correlation distance that gives an equivalent TOA shortwave change by neglecting height dependence of de-correlation length is about 0.4 km. Figure 4 shows that the variability of the correlation distance among for uppermost cloud top heights that are within ≈ 1 km of each other is on the order of 0.5 km. We expected that the 0.1 cloud fraction change is the upper bound, hence this tolerance value would be an underestimate for the following reason. Using $D_l = z_l - z_k$ in the estimate gives the largest cloud fraction change because a maximum of the function $\frac{z_l - z_k}{D_l^2} e^{-(z_l - z_k)/D_l}$ occurs when $z_l - z_k = D_l$. In addition, the the correlation distance varies with height more than that caused by the uppermost cloud top variation within ≈ 1 km (Figure 4), which is also an indication that neglecting height dependence has a larger effect on TOA irradiances.

Earlier studies indicate that the variability of TOA shortwave irradiance is mostly caused by the variability of the cloud fraction exposed to space [*Loeb et al.* 2007]. The relationship among the uppermost cloud top, correlation distance, and cloud fraction suggests that the cloud fraction exposed to space changes by the correlation length and the cloud fraction in the vertical layers. In the above two-layer system, the effective cloud thickness D_l determines whether the fraction of clouds in the k layer vertically extends from the l layer or the clouds exposed to space to become the uppermost cloud layer k. The sensitivity of the cloud fraction expose to the space to the correlation distance is largest when the k and l layers are separated by the distance D_l.

Earlier studies (e.g. *Barker et al.* [2003]) indicate that the cloud fraction exposed to space largely depends on the assumed type of cloud overlap. Whether switching from the random to the maximum cloud overlap assumption can lead to a significant improvement in the TOA shortwave irradiance depends on the error in the correlation length and cloud fraction in the vertical layers. If errors in the correlation length and the cloud fraction in vertical layers are large, adopting a proper cloud overlap assumption may not significantly improve TOA irradiance estimates. The change in the cloud fraction exposed to space due to changing to the maximum/random cloud overlap assumption from the random cloud overlap assumption in a two cloud layer system is $\Delta P(z_k, z_{top,l}) = P(z_l)[1 - P(z_l)]e^{\frac{-z_l - z_k}{D_k}}$. This term is greater than the change in the cloud fraction exposed to space caused by the error in the correlation length if $\frac{z_i - z_j}{D_i^2}\Delta D_i$ is less than unity, which is possible as long as the error in the correlation distance does not exceed 100% near the cloud base. Similar to the above two-cloud layer example, if we use $P(z_l) = 0.25$ and $D_l = z_l - z_k$, the change in

the cloud fraction exposed to space due to changing the overlap assumption $\Delta P(z_k, z_{top,l})$ is 0.19.

The sensitivity of the cloud fraction exposed to space due to the error in the cloud fraction is

$$\frac{\partial P(z_k, z_{top,k})}{\partial P(z_k)} = 1 - \sum_{i=k+1}^{m} P(z_i, z_{top,i}). \tag{22}$$

The second term on the right side is the cloud fraction exposed to space above the kth layer. Comparing (22) with $\Delta P(z_k, z_{top,l}) = P(z_l)[1 - P(z_l)]e^{\frac{-z_l - z_k}{D_k}}$, if the cloud fraction error in the kth layer is smaller than the upper-layer cloud fraction in a two layer system, the error in the cloud fraction exposed to space due to the error in the cloud fraction is smaller than $\Delta P(z, z_{top})$. Therefore, the improvement of the TOA irradiance estimate caused by adopting a proper cloud overlap parameterization is large if the upper layer cloud fraction is large.

5. Summaries and Conclusions

We combined vertical cloud profile from CALIPSO and CloudSat to utilize the strength of each instrument and to understand vertical cloud profile quantitatively. We introduced the cloud frequency of occurrence matrix that contains the vertical cloud profile as a function of uppermost cloud top. When we assume that the cloud overlap approaches the random overlap as the distance between the two cloud layers increases and define the e-folding distance of the cloud occurrence probability deviating from the random overlap, the uppermost cloud top and the cloud fraction vertical profiles can be related. The e-folding distance, or correlation distance, is interpreted as the effective cloud thickness. Cloud vertical profiles derived from CALIOP and CPR shows that the cloud occurrence in

layers below the uppermost cloud layer deviating from the random overlap nearly decays exponentially. However, the data show that the correlation distance is not necessarily constant throughout the atmospheric column for a given uppermost cloud top height. A large correlation distance might be an indication of precipitation and the change of the correlation distance might be used to screen precipitation.

In a two-cloud layer system, the correlation distance is equivalent to the de-correlation distance introduced by *Hogan and Illingworth* [2003] when the upper and lower cloud fractions are the same. Therefore, the de-correlation distance, which appears to be a parameter somewhat unique to general circulation models, is linked to the effective cloud thickness.

Appendix A: The effect of the vertical bin size

If we assume the conditional probability of cloud occurrence decreases exponentially with the distance from the uppermost cloud top

$$p(z_j|z_{top,i}) = e^{-z_{ji}/D_i}, \tag{a1}$$

where $p(z_j|z_{top,i})$ is the probability of cloud occurrence in a thin layer and $z_{ji} = z_i - z_j$. The mean probability of cloud occurrence in the uppermost layer of Δz_i thickness is

$$P(z_i|z_{top,i}) = \frac{1}{\Delta z_i}\int_0^{\Delta z_i} e^{-z/D_i}dz = \frac{D_i(1-e^{-\Delta z_i/D_i})}{\Delta z_i}. \tag{a2}$$

When $\Delta z_i/D_i \ll 1$, $P(z_j|z_{top,i}) \approx 1$. The mean probability of cloud occurrence in the jth layer of which thickness is Δz_j and z_{ji} distance from the uppermost cloud top layer i is

$$P(z_j|z_{top,i}) = \frac{1}{\Delta z_j}\int_{z_{ji}-\Delta z_j/2}^{z_{ji}+\Delta z_j/2} e^{-z/D_i}dz = \frac{D_i e^{\frac{-z_{ji}}{D_i}}\left(e^{\frac{\Delta z_j}{2D_i}} - e^{\frac{-\Delta z_j}{2D_i}}\right)}{\Delta z_j}. \tag{a3}$$

The conditional probability then becomes

$$\frac{P(z_j|z_{top,i})}{P(z_i|z_{top,i})} = \frac{\Delta z_i e^{\frac{z_{ji}}{D}} \left(e^{\frac{\Delta z_j}{2D}} - e^{\frac{-\Delta z_j}{2D_i}} \right)}{\Delta z_j \left(1 - e^{\frac{-\Delta z_i}{D_i}} \right)}. \quad (a4)$$

When $\Delta z_j / D \ll 1$, the conditional probability is

$$\frac{P(z_j|z_{top,i})}{P(z_i|z_{top,i})} \approx e^{-z_{ji}/D_i}. \quad (a5)$$

293

Appendix B: The relation between cloud fraction and uppermost cloud top profiles

The conditional probability of the cloud occurrence in the jth layer given the uppermost cloud top is in the ith layer is the sum of the probability due to a random overlap and a maximum overlap,

$$P(z_j|z_{top,i}) = P(z_j) + [1 - P(z_j)] \exp\left[-(z_i - z_j)/D_i\right]. \quad (b1)$$

Because $P(z_j|z_{top,i})P(z_i, z_{top,i}) = P(z_j, z_{top,i})$ and $\sum_{i=j}^{m} P(z_j, z_{top,i}) = P(z_j)$, when we multiply (b1) by $P(z_i, z_{top,i})$ and sum up from $i = j$ to m, then

$$P(z_j) = \sum_{i=j}^{m} P(z_i, z_{top,i})P(z_j) + \sum_{i=j}^{m} P(z_i, z_{top,i})[1 - P(z_i)] \exp\left[-(z_i - z_j)/D_i\right]. \quad (b2)$$

294 This expression leads to (14).

Appendix C: Cloud merging and grouping process

295 The CALIPSO and CloudSat cloud masks, obtained from the VFM and CLDCLASS
296 products, respectively are independent and sometimes can differ significantly due to char-
297 acteristics of the instrument used. This allows three combinations when the CALIPSO

and CloudSat masks are paired: 1) CALIPSO is cloud-free in the column and CloudSat reports clouds, 2) CALIPSO reports clouds and CloudSat is cloud-free in the column, and 3) both CALIPSO and CloudSat report clouds somewhere in the column. If only one of the paired profiles is valid, the valid profile is used without altering the profile.

After identifying the three cloud mask combinations described above, the cloud masks are compared at each vertical layers from each instrument. The vertical resolution of CALIPSO profile is 30 m below the altitude of 8 km and 60 m above the altitude of 8 km [*Winker et al.* 2007]. The vertical resolution of CloudSat profile is 240 m throughout [*Stephens et al.* 2008]. Comparing the cloud masks layer by layer, identical profiles are grouped. Where both the CALIPSO and CloudSat profiles are cloudy, all CALIPSO profiles match and all CloudSat profiles match for it to be grouped together. If the number of resulting groups is less than 16, all groups are kept. If that number is exceeded, similar, less populous profiles are combined together until the number becomes less than or equal to 16.

The process to reduce the number of cloud groups when it exceeds 16 is as follows. First, the number of unique profiles within a case, CALIPSO cloudy CloudSat cloud-free profiles, CALIPSO cloud-free CloudSat cloudy profiles, and CALIPSO and CloudSat cloudy profiles, is determined by

$$n_j^f = 16 \frac{N_j^i}{\sum_{i=1}^{3} N_i^i} \frac{16}{\sum_{i=1}^{3} n_i^i}, \qquad (c1)$$

where N is the number of profiles in the case, n is the number of unique profiles in the case (i.e. N > n) and superscript i and f, respectively, indicate the initial and final. If the number of unique profiles in the case is within the limit, no combining is done for the case. If the limit is exceeded, all unique profiles that contain nine or more matches

are kept. Then starting with the remaining profile with the most exact matches, other profiles that only differ by one are combined with it. If this fails to reduce the number of profiles below the limit, the last step is repeated combining profiles that differ by an increasing number of layers until the limit is met.

The number of cloud profiles in a CERES footprint is sometimes nearly 50 (Figure 5). This cloud grouping process reduces the number of profiles to less than or equal to 16. The area covered by different cloud profiles grouped together is less than 10% for most of CERES footprints. As a result, the cloud profiles are not altered very much from the original CALIOP and CPR cloud profiles (Figure 6). The number of vertical layers in a profile before the algorithm reduces it to the maximum of 6 is less than 6 for most of merged profiles (Figure 7). 99.68

Acknowledgments. We thank Drs. David Winker, Charles Trepte, Mark Vaughan, Gerald Mace, Roger Marchand, and Robert Holz for helpful discussions. The work was supported by the NASA Science Mission Directorate through the NASA Energy Water Cycle Study (NEWS) project.

References

Barker, H. W. (2008a), Representing cloud overlap with an effective de-correlation length: An assessment using CloudSat and CALIPSO data *J. Geophys. Res.*, 113, D24205, dio:10.1029/2008JD010391.

Barker, H. W, (2008b), Overlap of fractional cloud for radiation calculation in GCMs: A global analysis using CloudSat and CALIPSO data, *J. Geophys. Res.*, 113, D00A01, dio:10.1029/2007JD009677.

Barker, H. W. and P. Päosänen, (2005), Radiative sensitivities for cloud structural properties that are unresolved by conventional GCMs *J. Q. R. Meteorol. Soc.*, 131, 3103-3122.

Barker, H. W., and co-authors, (2003), Assessing 1D atmospheric solar radiative transfer models: interpretation and handling of unresolved clouds, *J. Climate*, 16, 2676-2699.

Chang, F.-L., and Z. Li, (2005), A new method for detection of cirrus-overlapping-water clouds and determination of their optical properties. *J. Atmos. Sci.*, 62, 3993-4009.

Dong, X., B. A. Wielicki, B. Xi, Y. Hu, G. G. Mace, S. Benson, F. Rose, S. Kato, T. Charlock, and P. Minnis, (2008), Using observations of deep convective systems to constrain atmospheric column absorption of solar radiation in the optically thick limit, *J. Geophys. Res.*, 113, D10206, doi:10.1029/2007JD009769.

Hogan, R. J., and A. J. Illingworth, (2003), Parameterizing ice cloud inhomogeneity and he overlap of inhomogeneities using cloud radar data, *J. Atmos. Sci.,*, 60, 756-767.

Hogan, R. J., and A. J. Illingworth, (2000), Deriving cloud overlap statistics from radar, *Q. J. R. Meteorol. Soc.*, 126, 2903-2909.

Jacob, C., and S. A. Klein, (2000), A parameterization of the effect of cloud and precipitation overlap for use in general-circulation models, Q. J. R. Meteorol. Soc., 126, 2525-2544.

Kato, S, F. G. Rose, D. A. Rutan, and T. P. Charlock, (2008), Cloud effects on the meridional atmospheric energy budget estimated from Cloud and the Earth's Radiant Energy System (CERES) data, *J. Climate*, 21, 4223-4241.

Loeb, N. G. B. A. Wielicki, F. G. Rose, and D. R. Doelling (2007), Variability in global top-of-atmosphere radiation between 2000 and 2005, *Geophys Res. Lett*, 34, L03704, doi:10.1029/2006GL028196.

Mace, G. G., and S. Benson-Troth, (2002), Cloud-layer overlap characteristics derived from long-term cloud radar data, *J. Climate*, 15, 2505-2515.

Minnis, P., J. Huang, B. Lin, Y. Yi, R. F. Arduini, T.-F. Fan, J. K. Ayers, and G. G. Mace (2007), Ice cloud properties in ice-over-water cloud systems using TRMM VIRS and TMI data, *J. Geophys. Res.*, 112, D06206, doi:10.1029/2006JD007626.

Smith, G. L. (1994), Effects of time response on the point spread function of a scanning radiometer, *Appl Opt.*, 30, 7031-7037.

Stephens, G. L. and co-authors, (2002), The CloudSat mission and a-train, *Bull. Amer. Meteor. Soc.*, 83, 1771-1790.

Stephens, G. L., and co-authors, (2008), CloudSat mission: performance and early science after the first year of operation, *J. Geophys. Res.*, 113, D00A18, doi:10.1029/2008JD009982.

Wang, L., and A. E. Dessler, (2006), Instantaneous cloud overlap statistics in the tropical area revealed by ICESat/GLAS data, *Geophys. Res. Lett.*, 33, L15804, doi:10.1029/205GL024350.

Willén, Ulrika, S. Crewell, H. K. Baltink, and O. Sievers, (2005), Assessing model predicted vertical cloud structure and cloud overlap with radar and lidar ceilometer observations for the Baltex Bridge Campaign, *Atmos. Res.*, 75, 227-255.

Winker, D. M., W. H. Hunt, and M. J. Mcgill, (2007), Initial performance assessment of CALIOP, *Geophys. Res. Lett.*, 34, L19803, doi:10.1029/2007GL030135.

Table 1. Cloud mask merging strategy

Cloud boundary	CALIOP	CPR	Merged boundary
Top	Detected	Detected	Higher cloud top
Top	Detected	Undetected	CALIOP cloud top
Top	Undetected	Detected	CPR cloud top
Base	Not completely attenuated	Undetected	CALIOP cloud base
Base	Not completely attenuated	Detected	CALIOP cloud base
Base	Completely attenuated	Detected	CPR cloud base
Base	Completely attenuated	Undetected	CALIOP lowest unattenuated base

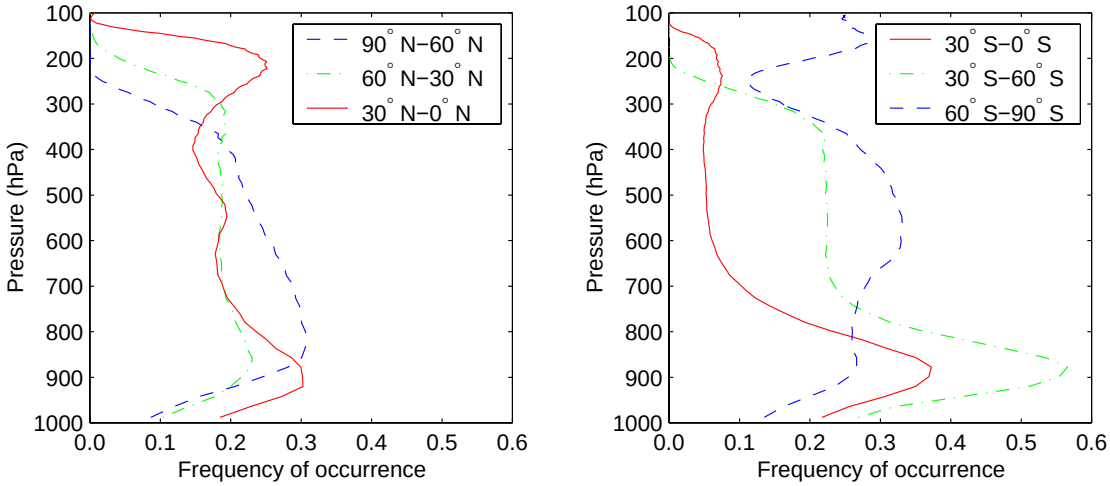

Figure 1. Cloud faction vertical profile derived from CALIPO and CPR merged cloud profiles computed with 200 m resolution for July 2006. left) northern hemisphere and right) southern hemisphere.

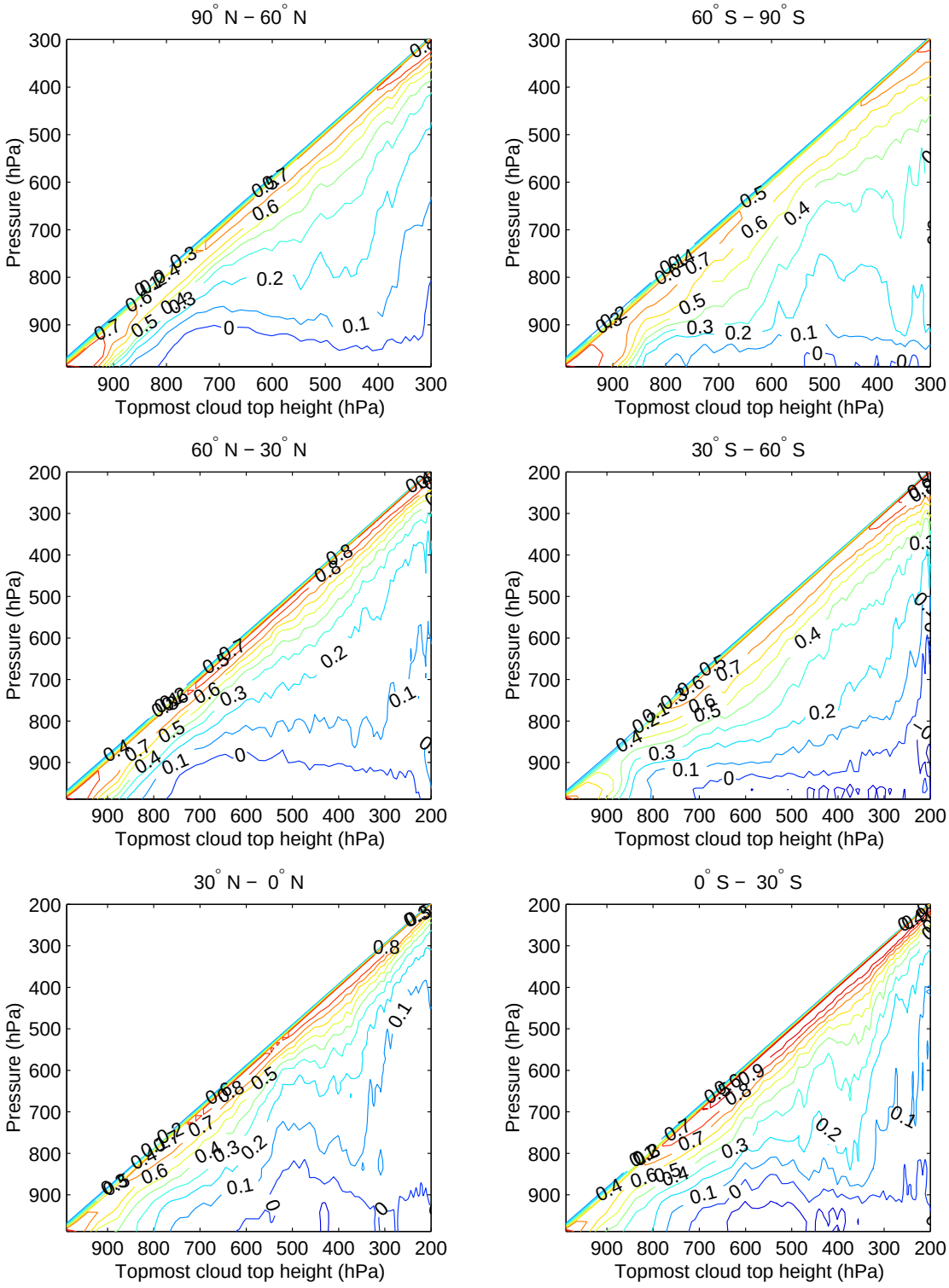

Figure 2. Deviation from the random overlap ΔP defined in (9) as a function of uppermost cloud top height for 6 different regions. Cloud vertical profiles derived from July 2006 CALIOP and CPR data are used.

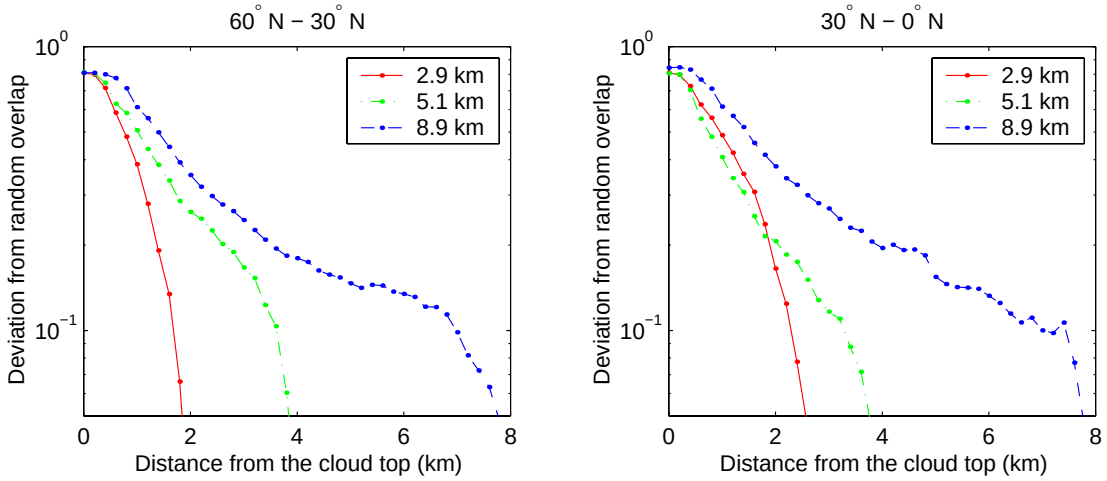

Figure 3. Deviation from the random overlap ΔP as a function of distance from the uppermost cloud top for three uppermost cloud top heights.

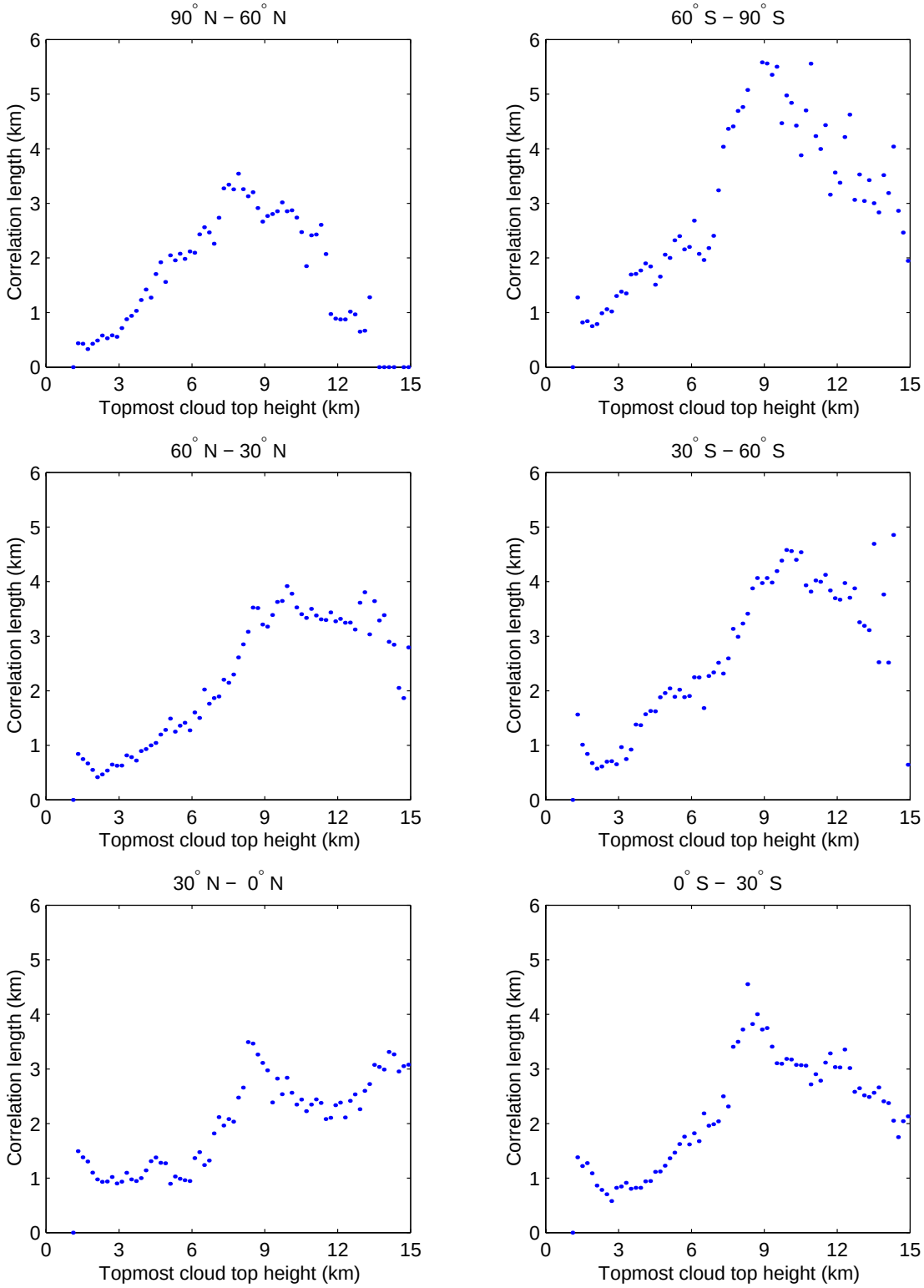

Figure 4. Correlation length derived from one month (July 2006) of CALIOP and CPR of data as a function of uppermost cloud top height for 6 different regions.

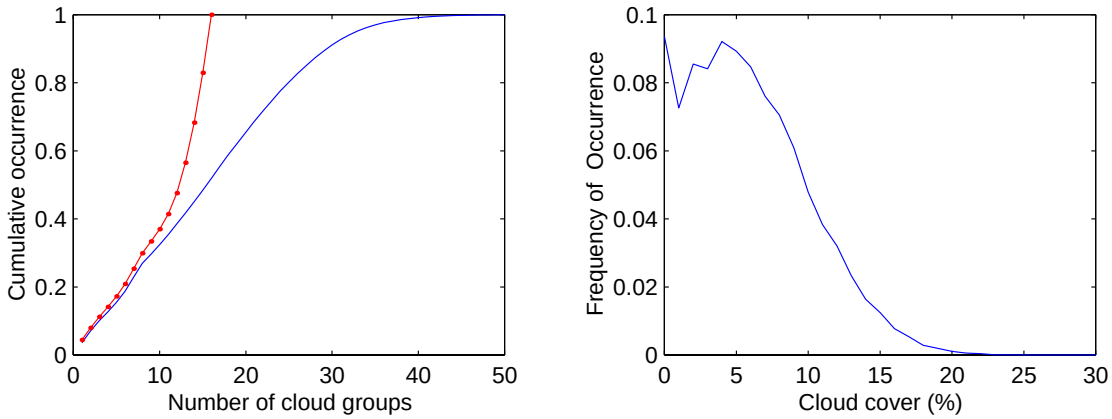

Figure 5. Left) Cumulative distribution of the number of cloud groups in a CERES footprint. The blue line indicates the actual number of profile cumulative distribution and the red line indicates the cumulative distribution after reducing to the maximum of 16 groups in a footprint. Right) Cloud fraction of cloud groups greater than or equal to the 11th cloud group number. The cloud group number having the largest cloud fraction over a footprint is 1 and the largest cloud number is assigned to the cloud group having he smallest cloud fraction.

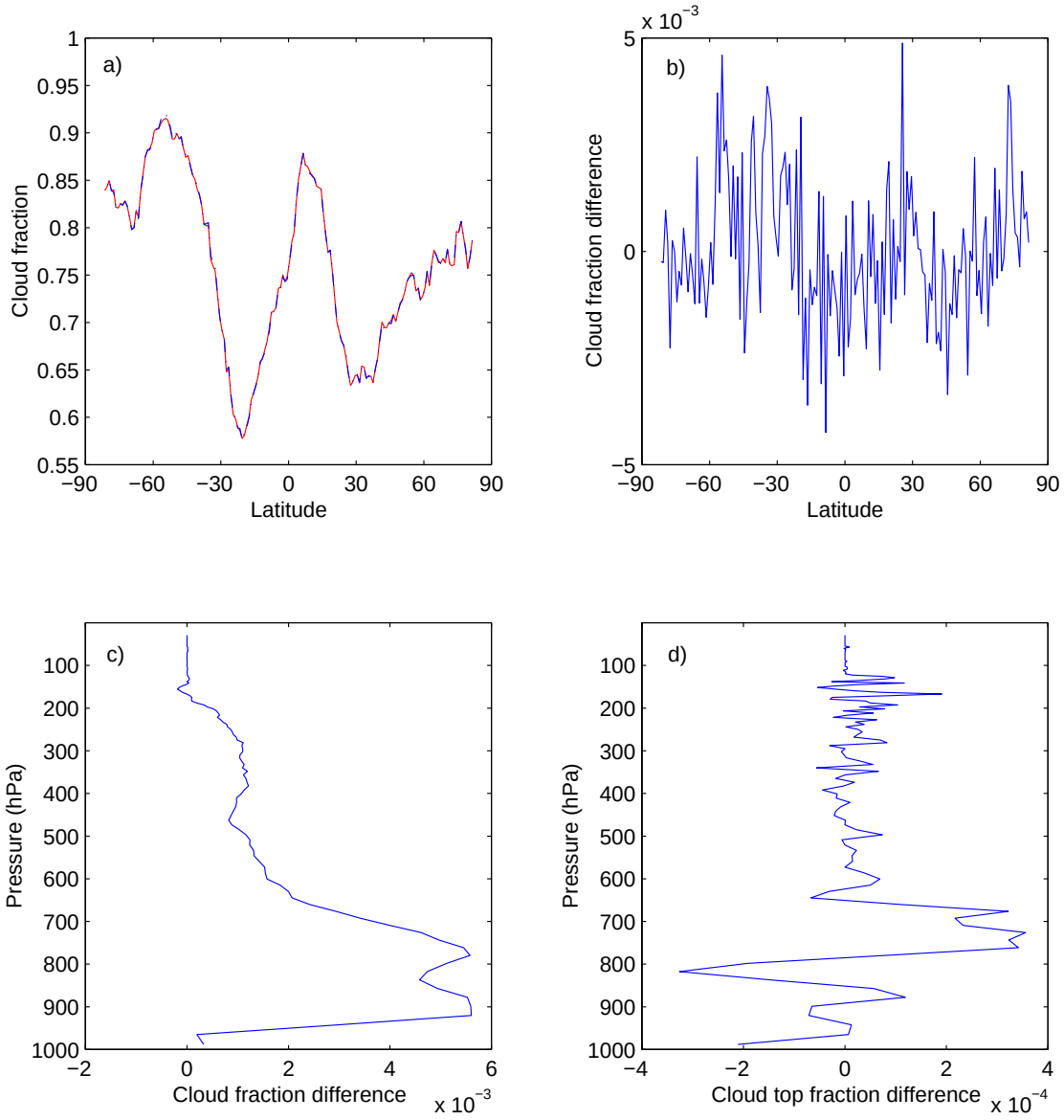

Figure 6. a) Cloud fraction exposed to space as a function of latitude derived from CALIPSO-CloudSat merged cloud profile before grouping (solid line) and after grouping (dash-dot line). The difference (after grouping minus before grouping) of the zonal mean cloud fraction exposed to space b), the difference in the cloud fraction vertical profile c), and uppermost cloud top fraction vertical profile d).

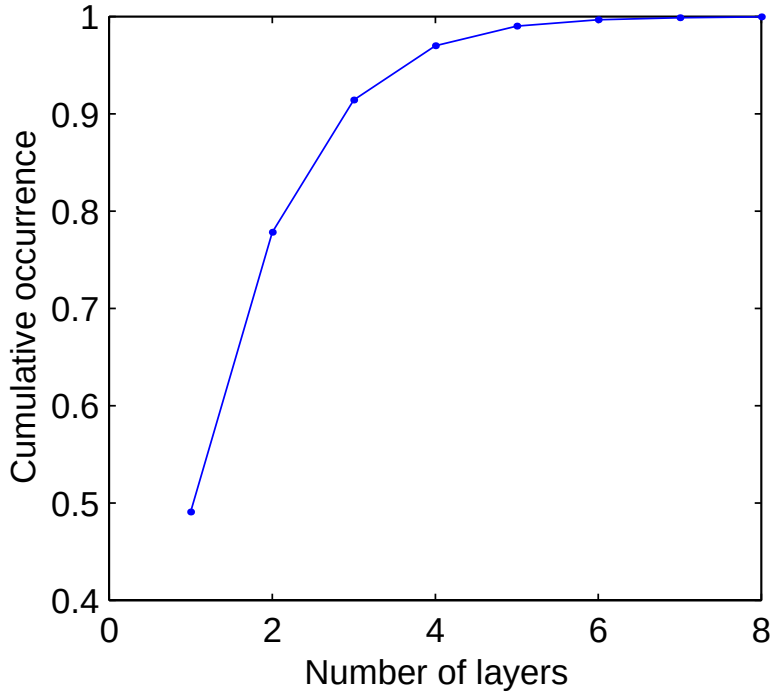

Figure 7. Cumulative occurrence of the number of vertical cloud layers in a CALIPSO-CloudSat merged cloud profile.